JOURNAL OF SOLID STATE CHEMISTRY **127,** 178–185 (1996)
ARTICLE NO. 0374

Structural and Surface Properties of $Bi_3(MSb_2)O_{11}$ (M = Al, Ga)

Ismunandar and Brendan J. Kennedy

School of Chemistry, University of Sydney, New South Wales 2006, Australia

and

Brett A. Hunter

Australian Nuclear Science and Technology Organisation, Private Mail Bag 1, Menai, New South Wales 2234, Australia

Received February 27, 1996; in revised form August 19, 1996; accepted August 22, 1996

The structures of the two oxides $Bi_3(MSb_2)O_{11}$ (M = Al, Ga) have been refined by Rietveld-type analysis of combined powder neutron and X-ray synchrotron diffraction data. The two oxides are isostructural, space group $Pn\bar{3}$, a = 9.43323(4) Å for M = Al and a = 9.48980(3) Å for M = Ga, in which the M and Sb atoms are statistically distributed in a 12*g* site. The structures can be described as two interpenetrating networks: a $M_{2/3}Sb_{4/3}O_9$ array of edge-sharing octahedra and a Bi_2O_3 array of corner-sharing Bi_8O_4 stellae quadrangulae. There are two independent Bi sites, both having distorted coordination geometries. The surface composition of both oxides is essentially identical to that of the bulk. Comparison with previous studies suggests that there may be some coupling between the mobility of the Bi ions in these oxides and their electronic properties.

INTRODUCTION

The two oxides $Bi_3(MSb_2)O_{11}$ (M = Al, Ga) are reported to be isostructural with $Bi_3Ru_3O_{11}$, space group $Pn\bar{3}$, and adopt a structure related to the cubic KSO_3-type structure (1). A recent study of the structural and electrocatalytic properties of the metallic oxide $Bi_3Ru_3O_{11}$ revealed two interesting, and possibly related, phenomena. First, the surface of the material was enriched in Bi, presumably as a consequence of diffusion of Bi ions in the large Bi_2O_3-type channels. Second, the thermal displacements of the Bi centers are both large and highly anisotropic (2–4). It can be supposed that surface enrichment requires Bi mobility and that this is reflected in the large thermal parameters.

A previous, low-resolution, structural study of $Bi_3(GaSb_2)O_{11}$ by Sleight and Bouchard (1) revealed two interesting anomalies; first, the coordination geometry of the $(M_{2/3}Sb_{4/3})O_9$ moieties was extremely distorted, the M–O bond lengths vary between 1.89 and 2.098 Å, and second, the isotropic thermal parameters of the two independent Bi sites were unusually large. If the latter observation is confirmed then it is feasible that unusual surface properties would also be observed in the two $Bi_3(MSb_2)O_{11}$ oxides.

As part of an ongoing study of the structural properties of catalysts, we have determined the structures of the two nonmetallic oxides $Bi_3(MSb_2)O_{11}$ (M = Al, Ga) using combined powder neutron and X-ray synchrotron diffraction and examined their surface properties. The results of these studies are described in this paper.

EXPERIMENTAL

$Bi_3(GaSb_2)O_{11}$ and $Bi_3(AlSb_2)O_{11}$ were prepared by the solid-state reaction of stoichiometric amounts of Bi_2O_3 (Aldrich, 99.999%), Al_2O_3 (BDH, 99.9%), Ga_2O_3 (Aldrich, 99.99%), and Sb_2O_3 (Aldrich, 99.999%) at 800°C for 24 h and then at 1100°C for 48 h [for $Bi_3(AlSb_2)O_{11}$] and at 900°C for the following 24 h and finally at 1050°C for 48 h [for $Bi_3(GaSb_2)O_{11}$], with regrinding after each heating step. Preliminary X-ray powder diffraction (XRD) measurements were recorded on a Siemens D-5000 diffractometer and showed the materials to be single phase. Scanning electron microscopy (SEM) and energy-dispersive X-ray analyses (EDS) were performed on a Phillips SEM 505 microscope equipped with an EDAX PV9900 energy-dispersive analyzer. X-ray photoelectron spectra were recorded on a Kratos XSAM 800 spectrometer using MgKα radiation (1254.6 eV), 10 mA,15 kV. Spectra were analyzed using a pseudo-Voigt peak shape function and a linear background.

The neutron powder diffraction (NPD) patterns were recorded at room temperature using neutrons of wavelength 1.4928 Å and 0.05° steps in the range $0° < 2\theta < 156°$ on the high-resolution powder diffractometer (HRPD) (5) on the HIFAR reactor operated by Australian Nuclear

0022-4596/96 $18.00

Science and Technology Organisation. The lightly ground sample was contained in a thin-walled 16-mm-diameter vanadium can that was slowly rotated during the measurement to minimize the effects of preferred orientation. The room temperature synchrotron XRD patterns were recorded at a wavelength of 0.99756 Å in 0.010045° steps in the range $5° < 2\theta < 165°$ on the Australian National Beamline Facility (ANBF) powder diffractometer, BL-20B, at the KEK Photon Factory, Japan. The data were collected using four image plates as the detectors covering the angular ranges 5–45°, 45–85°, 85–125°, and 125–165°. The finely ground sample was housed in a 0.5-mm-diameter glass capillary and was rotated during the measurements. A full description of the diffractometer and the use of the image plate detectors has been given previously (6–8).

The Rietveld refinements (9) were undertaken with a version of the computer program LHPM (10) operating on a PC. LHPM has been modified for combined X-ray and neutron refinements and can handle multiple data sets with independent scale factors, background functions, and zero corrections. An absorption correction using the algorithm of Sabine and Dwiggins (11, 12) has been included. The background was defined by a fourth-order polynomial in 2θ and was refined simultaneously with the other profile parameters. A Voigt function was chosen to generate the lineshape of the neutron diffraction patterns and a pseudo-Voigt was employed for the X-ray data. In the case of the pseudo-Voigt function the width is defined by the usual function $(\mathrm{FWHM})^2 = U \tan^2\theta + V \tan\theta + W$, where U, V, and W are refinable parameters (13). For the Voigt the Gaussian component varied as $(\mathrm{FWHM})^2 = U \tan^2\theta + V \tan\theta + W$ and the width of Lorentzian component was varied as $\eta \sec\theta$ to model particle size. The coherent neutron scattering lengths used were Bi = 0.853, Al = 0.345, Ga = 0.729, Sb = 0.546, O = 0.580 fm (10^{-15}m) (14). Appropriate scattering factors, f' and f'', were used for analysis of the XRD data. Initially the neutron and X-ray data were treated independently, and the structural parameters reported by Sleight and Bouchard (1) for $Bi_3(GaSb_2)O_{11}$ were used as a starting model. In the final structural refinement from the neutron diffraction data 40 parameters were varied, including 7 positional and 20 anisotropic thermal parameters. For the independent structural refinement from the XRD data, isotropic thermal parameters were employed and a total of 43 parameters varied. The final positional parameters and various measures of fit for $Bi_3(GaSb_2)O_{11}$ from the two independent refinements are given in Table 1. In both cases the refined parameters are in reasonably good agreement with the earlier study of Sleight and Bouchard (1). Similar results were obtained for $Bi_3(AlSb_2)O_{11}$, although for the sake of brevity these are not reported here. At this stage structural refinement using the combined XRD and NPD data sets was carried out for both materials. In each case the combined data set contained about 19,000 data points and 1500 reflections. In the refinements 73 parameters were varied. The profile functions used were the same as those used for the individual refinements. The final parameters for both compounds are listed in Table 2.

RESULTS AND DISCUSSION

The preparation of highly crystalline, pale yellow monophasic samples proceeded without incident. Preliminary XRD measurements did not reveal any obvious impurities, an observation confirmed in the higher-resolution synchrotron XRD study. The electron micrographs demonstrated that both materials were highly crystalline, with no anomalous features being observed. The homogeneity of the sample was verified using EDS analysis, which also showed that the bulk composition of both materials was as expected. The final positional and thermal parameters for the two oxides obtained by refinement from the combined NPD and XRD data sets are given in Table 2, and selected interatomic distances are listed in Table 3. The final observed, calculated, and difference profiles for $Bi_3(AlSb_2)O_{11}$ are shown in Fig. 1. It is obvious from Table 2 that the combined refinements have afforded extremely precise structural parameters. While the stated ESDs are pleasingly small, it must be recalled that the ESDs are solely a measure of the statistical precision of the parameters and strictly are not a measure of accuracy. Furthermore, it is well known that the Rietveld method tends to overstate the precision in the lattice parameter determination (15). This is particularly true in the present case where the errors associated with the calibration of the neutron and X-ray wavelengths have been neglected. It is also well recognized that a major shortcoming of Rietveld-type refinements of powder diffraction data is that, as a consequence of the loss of the directional character in reciprocal space, a single experiment need not necessarily yield the unique correct answer. A model that satisfactory reproduces both the XRD and NPD data is more likely to be accurate.

Initially the synchrotron diffraction data were collected as one of a number of measurements used to characterize the new high-resolution powder diffractometer at the ANBF (7, 8). In a related study of TiO_2, we found excellent agreement between the results of refinements from powder synchrotron XRD and NPD data (8). Consequently it was anticipated that the XRD and NPD studies of the present compounds would afford similar results. Thus it is observed for $Bi_3(GaSb_2)O_{11}$ that the refined positional parameters for the ''heavy'' atoms, Bi, Sb, and Ga/Al, lie within three combined ESDs in the three refinements (Tables 1 and 2). This is also true for O(1), which is at an 8*e* site having ($x = y = z$), where x is found to be 0.1474(2), 0.1485(7), and 0.1477(3) from the neutron, synchrotron X-ray, and combined refinements, respectively. For O(2), located at

TABLE 1
Positional Parameters for $Bi_3(GaSb_2)O_{11}$ from Independent Refinements from Neutron and X-ray Synchrotron Data

	Neutron (R_p = 4.54%, R_{wp} = 5.54%)			X-ray (R_p = 2.44%, R_{wp} = 4.29%)		
Atom	*x*	*y*	*z*	*x*	*y*	*z*
Bi(1)	0.3802(1)[a]	*x*	*x*	0.38008(7)	*x*	*x*
Bi(2)	0	0	0	0	0	0
Ga/Sb	0.5920(2)	0.7500	0.2500	0.59260(7)	0.7500	0.2500
O(1)	0.1474(2)	*x*	*x*	0.1485(7)	*x*	*x*
O(2)	0.6118(2)	0.2500	0.2500	0.6179(9)	2500	0.2500
O(3)	0.5894(2)	0.5387(2)	0.2455(2)	0.5873(5)	0.5362(5)	0.2381(6)

[a] Values in parentheses are the e.s.d.'s in the last significant digits.

the 12*f* site (*x*, 0.25, 0.25) and, to a much lesser extent O(3), there appears to be significant differences between the results obtained in the structural refinements from the XRD and NPD data, *x* for O(2) being 0.6118(2) and 0.6179(9), respectively. It must be stressed that irrespective of the starting positional parameters the refinements always converged to the above values. The oxygen positional parameters obtained in the joint refinement are intermediate between those obtained from the independent XRD and NPD refinements. Thus, the difference does not appear to be due simply to the failure of the XRD data to locate these atoms, but rather suggests that there is a small displacement of the electron density around O(2). The apparent displacement of O(2) corresponds to a contraction of the Ga/Sb–O(2) distance by ca. 0.01 Å in the X-ray diffraction study and a similar expansion in the Bi(1)–O(2) distance. An identical effect is observed for $Bi_3(AlSb_2)O_{11}$, where analysis of the diffraction data suggests there is a small displacement of the O(2) atom, all other atomic coordinates being in good agreement in the two analysis. It is possible that this difference is a consequence of polarization of the electron cloud at O(2). In the terms of the local bonding such a polarization may be a consequence of the directional nature of the *M*–O(2)–*M* bonding interactions. Single-crystal measurements using both X rays and neutrons are required to confirm this.

TABLE 2
Atomic Coordinate and Isotropic and Anisotropic Thermal Parameters (10^3 Å^2) for $Bi_3(GaSb_2)O_{11}$ and $Bi_3(AlSb_2)O_{11}$ at Room Temperature Obtained from Refinement from the Combined X-ray and Neutron Powder Diffraction Data

Atom	Site	*x*	*y*	*z*	B_{iso}[a]	u_{11}	u_{22}	u_{33}	u_{12}	u_{13}	u_{23}
$Bi_3(AlSb_2)O_{11}$, $Pn\bar{3}$, *a* = 9.43323(4) Å, R_p = 2.65%, R_{wp} = 4.18%											
Bi(1)	8*e* (*x*, *x*, *x*)	0.38065(4)[b]	*x*	*x*	2.99(6)	37.92(2)	u_{11}	u_{11}	−15.3(9)	u_{12}	u_{12}
Bi(2)	4*b* (0, 0, 0)	0	0	0	2.02(6)	25.1(1)	u_{11}	u_{11}	−5.4(9)	u_{12}	u_{12}
Al1/3Sb2/3	12*g* (*x*, 3/4, 1/4)	0.59384(6)	0.7500	0.2500	0.34(4)	5.2(2)	4.1(3)	2.4(3)	0	0	0.9(3)
O(1)	8*e* (*x*, *x*, *x*)	0.1472(3)	*x*	*x*	0.54(4)	8.2(9)	u_{11}	u_{11}	−5.0(9)	u_{12}	u_{12}
O(2)	12*f* (*x*, 1/4, 1/4)	0.6164(4)	0.2500	0.2500	0.83(3)	0(2)	12(2)	19(2)	0	0	9(2)
O(3)	24*h* (*x*, *y*, *z*)	0.5907(3)	0.5382(3)	0.2465(4)	0.48(2)	3(1)	5.0(9)	1.9(2)	3.6(9)	−11(1)	0(1)
$Bi_3(GaSb_2)O_{11}$, $Pn\bar{3}$, *a* = 9.48980(3) Å, R_p = 2.07%, R_{wp} = 3.65%											
Bi(1)	8*e* (*x*, *x*, *x*)	0.37995(4)	*x*	*x*	3.18(5)	42.4(2)	u_{11}	u_{11}	−17.5(2)	u_{12}	u_{12}
Bi(2)	4*b* (0, 0, 0)	0	0	0	2.00(4)	30.6(2)	u_{11}	u_{11}	−6.6(2)	u_{12}	u_{12}
Ga1/3Sb2/3	12*g* (*x*, 3/4, 1/4)	0.59247(6)	0.7500	0.2500	0.52(2)	5.5(2)	5.8(3)	0.8(2)	0	0	3.2(2)
O(1)	8*e* (*x*, *x*, *x*)	0.1477(3)	*x*	*x*	0.76(3)	11.2(9)	u_{11}	u_{11}	−5.0(9)	u_{12}	u_{12}
O(2)	12*f* (*x*, 1/4, 1/4)	0.6124(4)	0.2500	0.2500	1.00(3)	2(1)	15(2)	18(2)	0	0	17(2)
O(3)	24*h* (*x*, *y*, *z*)	0.5883(3)	0.5389(3)	0.2465(2)	0.66(2)	3.6(9)	8.5(9)	1.3(1)	3.2(9)	−9.9(9)	0(1)

[a] Values obtained for a refinement using isotropic thermal parameters. The inclusion of anisotropic thermal parameters did not significantly alter the structural and unit cell parameters.

[b] Values in parentheses are e.s.d.'s in the last significant digits.

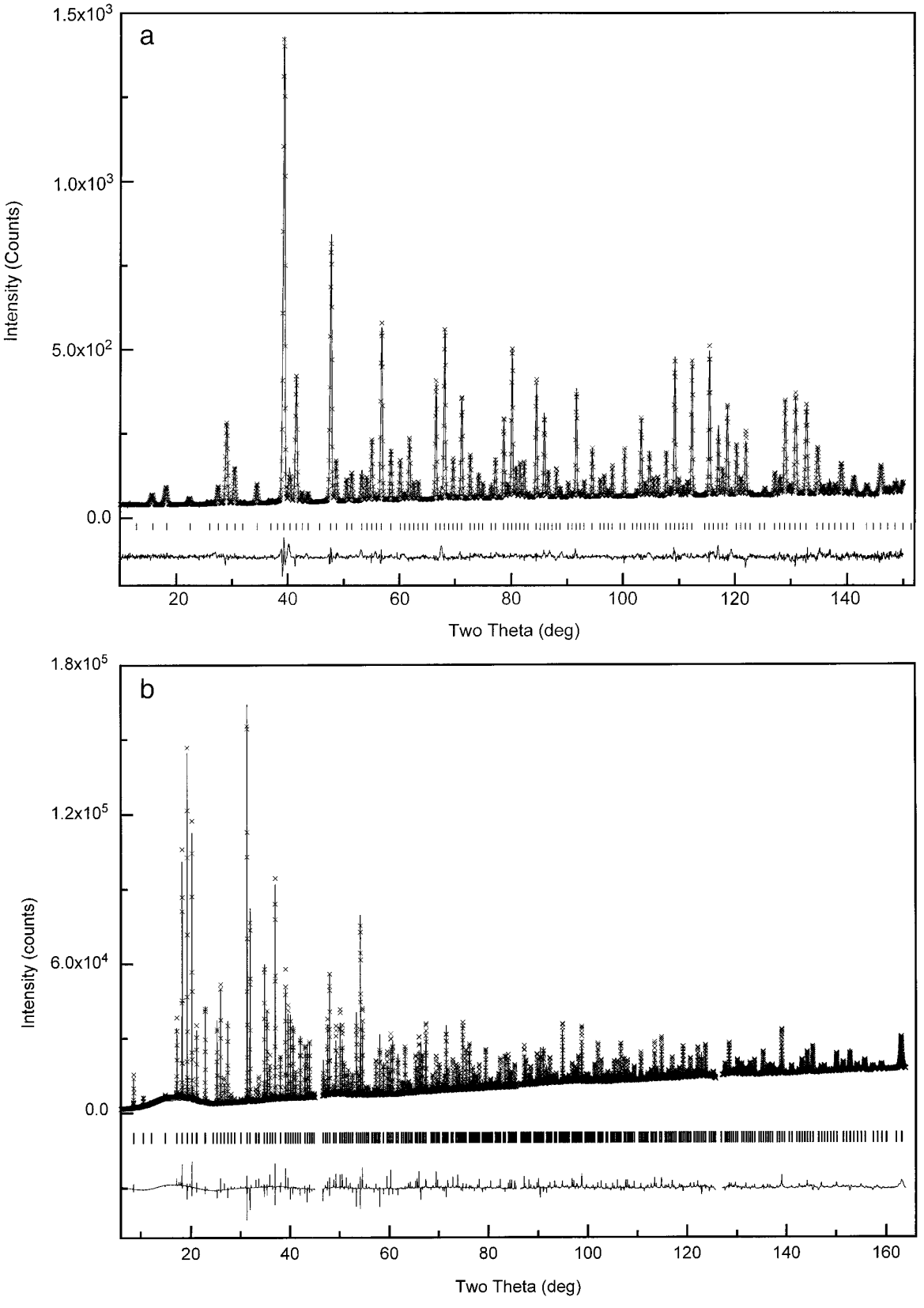

FIG. 1. Observed, calculated, and difference neutron powder (a) and X-ray synchrotron diffraction (b) profiles for $Bi_3(AlSb_2)O_{11}$. The observed data are indicated by crosses and the profiles calculated by the combined refinement of the X-ray and neutron data by the solid line. The short vertical lines below the profiles mark the positions of all possible Bragg reflections. The breaks that appear in the XRD pattern result from the small physical gap that occurs between the four image plate detectors.

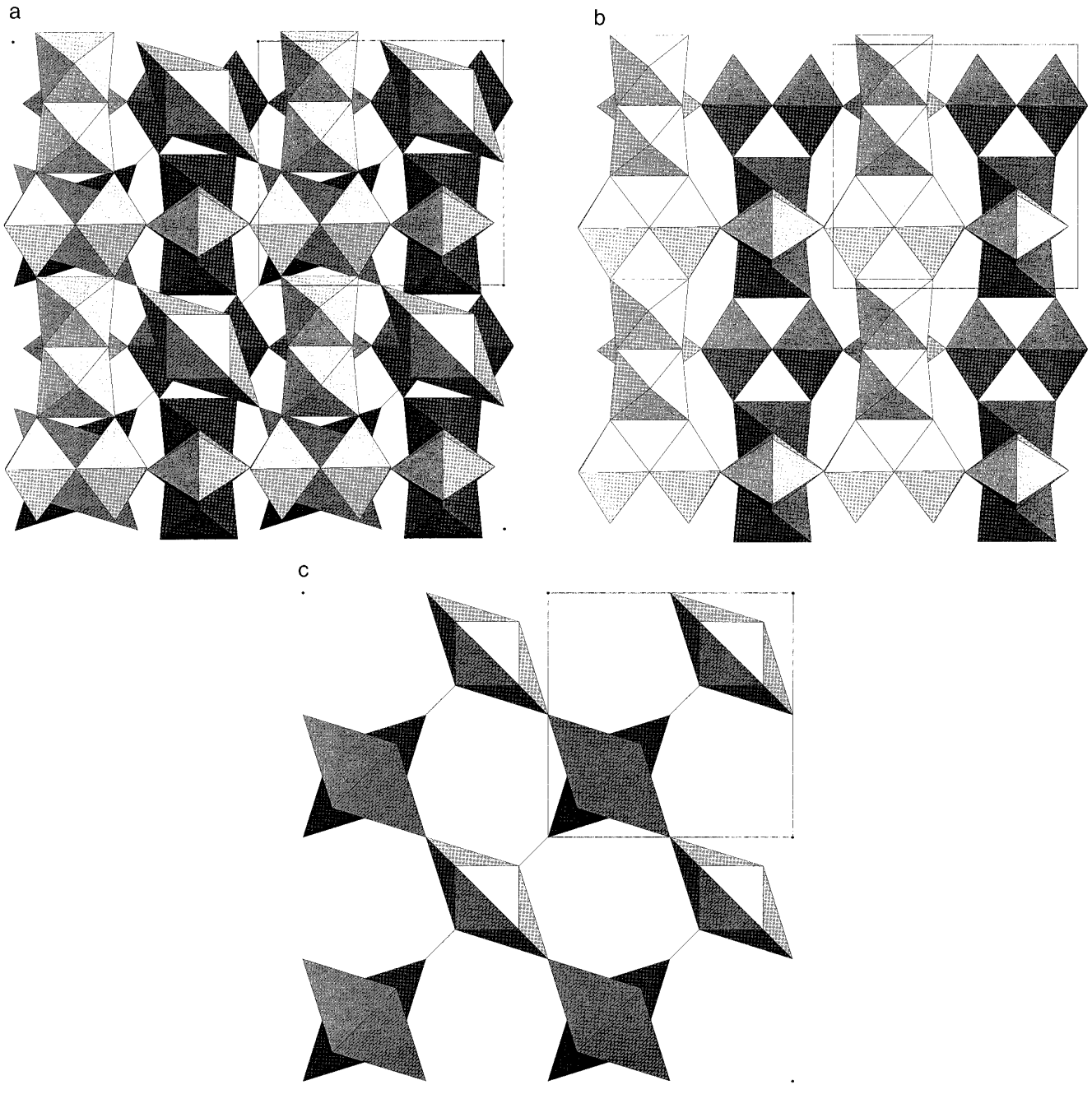

FIG. 2. (a) The structure of $Bi_3(MSb_2)O_{11}$ as two interpenetrating networks b and c. (b) View of the $M_{1/3}Sb_{2/3}O_3$ framework built from edge-sharing $M_{2/3}Sb_{4/3}O_{10}$ pairs further linked by vertex sharing. (c)Representation of the Bi_2O_3 framework built of corner-sharing Bi_8O_4 stellae quadrangullae.

The structure of the two oxides (Fig. 2a) can be described as two interpenetrating networks of a $(MSb_2)O_9$ array of pairs of edge-sharing octahedra (Fig. 2b) and a Bi_2O_3 array of corner-sharing Bi_8O_4 stellae quadrangulae (Fig. 2c).

In the present structure the M and Sb atoms are surrounded by six oxygens at distances ranging from 1.949 to 2.006 Å. The mean $\langle M/Sb–O\rangle$ distances are 1.969 Å and 1.989 Å for M = Al or Ga, respectively. The longer distance in the latter case reflects the larger ionic radii of Ga^{3+} versus Al^{3+} (16), a feature that is also apparent in the values of the lattice parameters, 9.43323(4) versus 9.48980(3) Å. The corresponding MO_6 polyhedra are slightly distorted octahedra (Table 3). The present refinement demonstrates that the coordination around the Al/Sb and Ga/Sb sites are more regular than that found previously (1). This result is, in part, a consequence of the considerably improved

TABLE 3
Selected Interatomic Distance (Å) for $Bi_3(AlSb_2)O_{11}$ and $Bi_3(GaSb_2)O_{11}$

$Bi_3(AlSb_2)O_{11}$		$Bi_3(GaSb_2)O_{11}$			
Bond	Distance (Å)[b]	Bond	Distance (Å)[b]	Distance (Å)[c]	Distance (Å)[d]
Bi(1)–O(1)	2.234(3)[e] 3×	Bi(1)–O(1)	2.235(3) 3×	2.240(1) 3×	2.34 3×
Bi(1)–O(2)	2.813(3) 3×	Bi(1)–O(2)	2.812(3) 2×	2.808(2) 2×	2.73 3×
Bi(1)–O(3)	2.782(3) 3×	Bi(1)–O(3)	2.792(3) 3×	2.800(1) 3×	2.77 3×
Bi(2)–O(1)	2.405(3) 2×	Bi(2)–O(1)	2.427(3) 2×	2.423(2) 2×	2.24 2×
Bi(2)–O(3)	2.504(3) 6×	Bi(2)–O(3)	2.512(3) 6×	2.507(2) 6×	2.53 6×
Al/Sb–O(2)	1.952(3) 2×	Ga/Sb–O(2)	1.985(3) 2×	1.992(1) 2×	2.05 2×
Al/Sb–O(3)	1.998(3) 2×	Ga/Sb–O(3)	2.003(3) 2×	2.006(1) 2×	2.098 2×
Al/Sb–O(3)	1.949(3) 2×	Ga/Sb–O(3)	1.977(3) 2×	1.965(2) 2×	1.89 2×

[a] In the case of $Bi_3(GaSb_2)O_{11}$, the results obtained from the three refinements discussed in the text are given.
[b] Calculated from combined refinement results.
[c] Calculated from neutron data refinement result.
[d] Calculated from Ref. (1).
[e] Values in parentheses are e.s.d.'s in the last significant digits.

accuracy and precision obtained in the current estimates of the various oxygen positional parameters.

Each $M_{1/3}Sb_{2/3}O(2)_2O(3)_4$ octahedron shares its O(2) edge with another octahedra to form a $M_{2/3}Sb_{4/3}O_{10}$ unit. In these units the metal–metal distances across the shared edge octahedra are 2.947 Å for $Bi_3(AlSb_2)O_{11}$ and 2.989 Å for $Bi_3(GaSb_2)O_{11}$; for perfect octahedra these distances would be 2.783 and 2.811 Å, respectively. Thus, it is apparent that in these insulating oxides the M/Sb metals are displaced away from each other. A similar effect is also observed in $La_3Ir_3O_{11}$ (17), and this is in contrast to the situation found in the metallic oxides $Bi_3Ru_3O_{11}$ (4) and $La_4Re_6O_{19}$ (18), where the two metals are displaced toward each other (Table 4). The $M_{2/3}Sb_{4/3}O_{10}$ units then share their eighth free O(3) corner with other units, forming a three-dimensional M_3O_9 network (Fig. 2b).

The Bi(1) atoms are coordinated to nine oxygen atoms forming a distorted tricapped trigonal prism (Fig. 3a, Table 3). There are two different bond lengths, three short bonds to O(1) at ca. 2.23 Å and six longer distances at ca. 2.8 Å to O(2) and O(3). If only the three short Bi(1)–O(1) bonds are considered, the coordination of Bi(1) can be described as a BiO_3 triangular pyramid closely related to those observed in sillenite $Bi_{12}(Bi_{0.5}Fe_{0.5})O_{19.5}$ (19) and Bi_2CdO_4 (20). The three strongly bonded oxygen atoms form the base and Bi(1) the apex of the pyramid. The Bi $6s^2$ lone pair electrons (E) are directed so as to constitute the fourth vertex of a BiO_3E tetrahedron. The three less strongly bonded O(3) atoms and the lone pair are located in the same side of bismuth atoms. This results in the triangular $O(3)_3$ face being much larger than the opposite $O(1)_3$ triangular face; the O(1)–O(1) distances are 2.743(4) and 2.747(4) Å for M = Al and Ga respectively, whereas the O(3)–O(3) distances are 4.282(4) and 4.292(4) Å for M = Al and Ga, respectively.

The Bi(2) atoms have an eightfold coordination geometry where the oxygen atoms are located at the corners of a compressed scalenohedron (Fig. 3b, Table 3). Two kinds of Bi(2)–O bond distances are observed, six long Bi(2)–O(2) distances and two somewhat shorter Bi(2)–O(1) distances. This coordination is the same as that observed in pyrochlore-type oxides such as $Bi_2M_2O_{7-y}$ M = Ru, Ir, Rh (4, 21). All the oxygen atoms are tetrahedrally coordinated to either Bi or (Bi and M/Sb). In both the $Bi(1)O_9$ and $Bi(2)O_8$ polyhedra the Bi–O(1) distances are systematically shorter than those distances to O(2) and O(3).

The short Bi(1)–O(1) and Bi(2)–O(1) distances result in arrays that can be described as units consisting of four $Bi(1)_3Bi(2)$ tetrahedra, each occupied by an O(1) anion,

TABLE 4
Metal–Metal Distances Across the Shared Edge in Some Related $A3B_3O_{11}$-Type Structures

Compound	Observed metal–metal distance (Å)	Metal–metal distance in perfect octahedra (Å)	Reference
$Bi_3(AlSb_2)O_{11}$	2.957(1)[a]	2.783	This work
$Bi_3(GaSb_2)O_{11}$	2.999(1)	2.811	This work
$Bi_3Ru_3O_{11}$	2.600(1)	2.792	(4)
$La_3Ir_3O_{11}$	2.981	2.814	(18)
$La_4Re_6O_{16}$	2.42	2.80	(16)

[a] Values in parentheses are e.s.d.'s in the last significant digits.

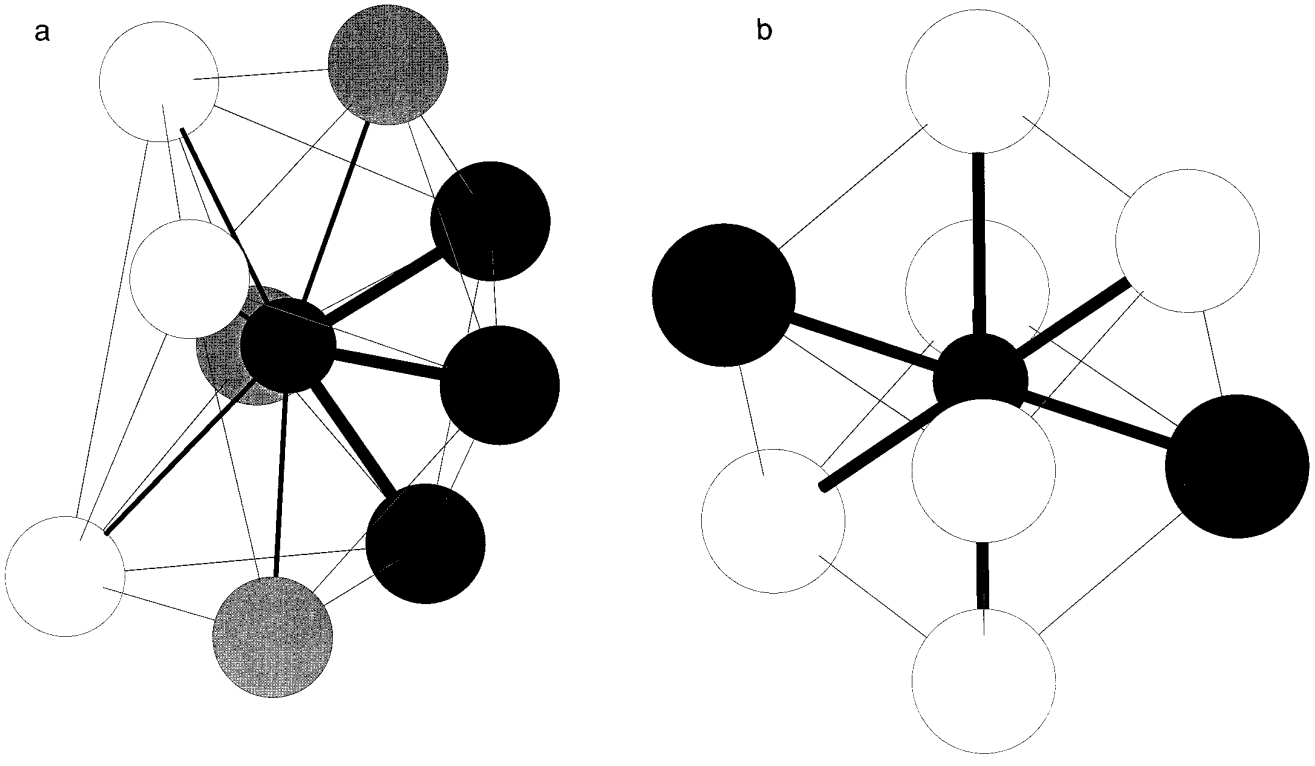

FIG. 3. (a) View of the tricapped trigonal prism of BiO_9. Note the pyramid formed by Bi(1) and $O(1)_3$ face. Open circles represent O(1), gray circles O(2), and black solid circles are O(3). (b) View of the $Bi(2)O_8$ compressed scalehedron. Open circles represent O(1) and black solid circles O(3).

and sharing their $Bi(1)_3$ face with an empty fifth $Bi(1)_4$ tetrahedral. Such $Bi(1)_4Bi(2)_4O(1)_4$ units can be described as an O(1)-filled Bi_8 stellae quadrangulae. These share their Bi(2) corners resulting in a three-dimensional framework of Bi_2O_3 (Fig. 2c), similar to corner-sharing stellae quadrangulae of Fe atoms observed in the zeta carbide W_3Fe_3C (22).

Bond valence sum calculations (23) gave the following results for $Bi_3(AlSb_2)O_{11}$ [Bi(1) = 2.9, Bi(2) = 2.8, Al/Sb = 4.3, O(1) = 2.5, O(2) = 1.8, O(3) = 1.8] and for $Bi_3(GaSb_2)O_{11}$ [Bi(1) = 2.9, Bi(2) = 2.8, Ga/Sb = 4.4, O(1) = 2.4, O(2) = 1.8, O(3) = 1.9]. Reliable crystal structure refinements usually gave calculated valences that agree to within 0.1–0.2 valence units with the theoretical values (24, 25), unless the compound contains significant distortions arising from steric or electronic effects. It is apparent in the present compounds that the overbonding of O(1) is exceptional. O(1) exists in $Bi(1)_3Bi(2)$ tetrahedra and the overbonding can be ascribed to the influence of the $6s^2$ lone-pair electrons of Bi(1), resulting in short Bi(1)–O(1) bonds.

The thermal parameters for the two types of Bi atoms are large and highly anisotropic. The Bi(2) atoms, which lie on a threefold axis, have two principal vibrations, $u_{11} + 2u_{12}$ parallel to (111) direction, and $u_{11} - u_{12}$, perpendicular to this. The value of these in $Bi_3(AlSb_2)O_{11}$ are 14.7×10^{-3} and 30.5×10^{-3} Å^2, whereas for $Bi_3(GaSb_2)O_{11}$ they are 17.4×10^{-3} and 37.2×10^{-3} Å^2 respectively, demonstrating that the movement along the threefold axis, i.e., toward the closest oxygen atoms is, as expected, strongly inhibited (26). In the case of Bi(1), which is coordinated to nine oxygen atoms, the smallest displacement corresponds to a movement toward the center of the face formed by the three O(1) atoms.

While the anisotropic nature of the Bi thermal parameters can be readily explained by consideration of the local bonding contacts, i.e., displacement toward the nearest oxygen atoms is inhibited, it is evident from Table 2 that the thermal parameters of the Bi atoms are appreciably larger than those of the lighter aluminum, gallium, antimony, and oxygen atoms. As found in $Bi_3Ru_3O_{11}$ (4) this appears to be a consequence of the fact that there is only weak interaction between Bi_2O_3 and M_2O_9 arrays. As stated in the Introduction it can be supposed that the large thermal motions are an indication of ionic mobility, and consequently surface segregation and/or enrichment might be anticipated. This, however, was not observed in an X-ray photoelectron spectroscopic study which showed the surface composition of the two materials to be essentially identical to that of the bulk. For $Bi_3(GaSb_2)O_{11}$ the diag-

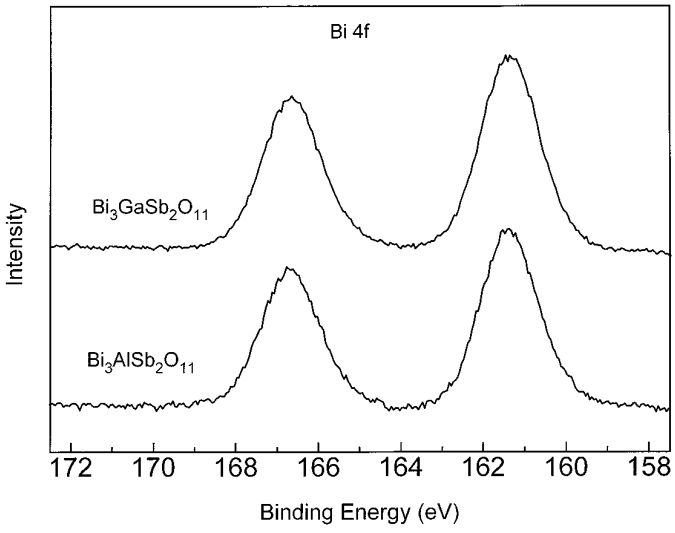

FIG. 4. Representative Bi 4*f* photoelectron spectra of $Bi_3(GaSb_2)O_{11}$ and $Bi_3(AlSb_2)O_{11}$. Note the broadening to lower binding energy as a consequence of X-ray-induced reduction.

nostic Bi 4*f*, Ga 3*d*, and Sb 3*d* lines all appeared as symmetrical spin-orbit doublets with binding energies typical of Bi^{3+}, Ga^{3+} and Sb^{5+}. In the case of $Bi_3(AlSb_2)O_{11}$ both the Sb 4*d* and Bi 4*f* signals were noticeably broadened to lower binding energies (Fig. 4), suggesting the presence of a second surface species. This asymmetry was observed to increase during the measurements and can be ascribed to beam-induced reduction that possibly results in surface recrystallization. The absence of appreciable surface segregation in these two materials contrasts with the results obtained for the metallic oxide, $Bi_3Ru_3O_{11}$, where the surface is Bi rich (4). This suggests there may be some coupling between the mobility of the Bi ions and the electronic properties of the materials. Further studies in this direction are in progress.

ACKNOWLEDGMENTS

This work has been supported by Australian Institute of Nuclear Science and Engineering, Australian Research Council, and Australian National Beamline Facility. We thank Dr. C. J. Howard (ANSTO) for useful discussions of this work. The assistance of Dr. Cookson and Dr. Foran at the ANBF is gratefully acknowledged.

REFERENCES

1. A. W. Sleight and R. J. Bouchard, *Inorg. Chem.* **12,** 2314 (1973).
2. G. Gokagac and B. J. Kennedy, *Langmuir* **9,** 1862 (1993).
3. G. Gokagac and B. J. Kennedy, *J. Electroanal. Chem.* **368,** 235 (1993).
4. G. R. Facer, M. M Elcombe, and B. J. Kennedy, *Aust. J. Chem.* **46,** 1897 (1993).
5. C. J. Howard, C. J. Ball, R. L. Davis, and M. M. Elcombe, *Aust. J. Phys.* **36,** 507 (1983).
6. Z. Barnea, D. C. Creagh, T. J. Davis, R. F. Garret, S. Janky, A. W. Stevenson, and D. C. Wilkins, *Rev. Sci. Instrum.* **63,** 1069 (1992).
7. R. F. Garret, D. J. Cookson, G. J. Foran, T. M. Sabine, B. J. Kennedy, and S. W. Wilkins, *Rev. Sci. Instrum.* **66,** 1351 (1995).
8. T. M. Sabine, B. J. Kennedy, R. F. Garrett, G. J. Foran, and D. J. Cookson, *J. Appl. Crystallogr.* **28,** 513 (1995).
9. H. M. Rietveld, *J. Appl. Crystallogr.* **2,** 65 (1969).
10. R. J. Hill and C. J. Howard, Australian Atomic Energy Commission Report No. M112, AAEC(now ANSTO), Lucas Heights Research Laboratories, New South Wales, Australia, 1986.
11. T. M. Sabine and W. R. Sabine, submitted for publication.
12. C. W. Dwiggins, *J. Appl. Crystallogr.* **13,** 572 (1980).
13. G. Caglioti, A. Paoletti, and F. P. Ricci, *Nucl. Instrum.* **3,** 223 (1958).
14. V. F. Sears, Atomic Energy of Canada Limited Report AECL-8490, 1984.
15. R. A. Young (Ed.), "The Rietveld Method." Oxford Science, Oxford 1993.
16. R. D. Shannon, *Acta Crystallogr.* **32,** 751 (1976).
17. F. Abraham, J. Trehoux, and D. Thomas, *J. Less. Common Met.* **63,** P57 (1979).
18. J. M. Longo and A. W. Sleight, *Inorg. Chem.* **7,** 108 (1968).
19. S. F. Radaev, L. A. Muradyan, and V. I. Simonov, *Acta Crystallogr.* B **47,** 1 (1991).
20. J. C. Champarnaud-Mesjard, B. Frit, A. Aftati, and M. ElFarisi, *Eur. J. Solid State Inorg. Chem.* **31,** 473 (1994).
21. B. J. Kennedy, *J. Solid State Chem.* **123,** 14 (1996).
22. B. G. Hyde and S. Anderson, "Inorganic Crystal Structures," p. 344. Wiley, New York, 1989.
23. N. E. Bresse and M. O'Keefe, *Acta Crystallogr. B* **47,** 192 (1991).
24. I. D. Brown, *Chem. Soc. Rev.* **7,** 359 (1978).
25. M. O'Keefe, *Structure Bonding* **71,** 161 (1989).
26. G. R. Facer, C. J. Howard, and B. J. Kennedy, *Powder Diffraction* **8,** 245 (1993).